Bioelectrochemistry 125 (2019) 46–57

Contents lists available at ScienceDirect

Bioelectrochemistry

journal homepage: www.elsevier.com/locate/bioelechem

The contribution of lipid peroxidation to membrane permeability in electropermeabilization: A molecular dynamics study

Lea Rems [a,*,1], Marilyne Viano [b], Marina A. Kasimova [b], Damijan Miklavčič [c], Mounir Tarek [b,*]

[a] Department of Chemical Engineering, Delft University of Technology, 2629 HZ, Delft, the Netherlands
[b] Université de Lorraine, CNRS, LPCT, F-54000 Nancy, France
[c] Faculty of Electrical Engineering, University of Ljubljana, Tržaška 25, SI-1000 Ljubljana, Slovenia

ARTICLE INFO

Article history:
Received 27 February 2018
Received in revised form 17 July 2018
Accepted 24 July 2018
Available online 04 August 2018

Keywords:
Electroporation
Oxidized lipids
Permeability
Electrical conductance
Cell membrane
Free energy calculations

ABSTRACT

Electroporation or electropermeabilization is a technique that enables transient increase in the cell membrane permeability by exposing cells to pulsed electric field. However, the molecular mechanisms of the long-lived cell membrane permeability, which persists on the minutes time scale after the pulse treatment, remain elusive. Experimental studies have suggested that lipid peroxidation could present a mechanism of this prolonged membrane permeabilization. In this study we make the first important step in quantifying the possible contribution of lipid peroxidation to electropermeabilization. We use free energy calculations to quantify the permeability and conductance of bilayers, containing an increasing percentage of hydroperoxide lipid derivatives, to sodium and chloride ions. We then compare our calculations to experimental measurements on electropermeabilized cells. Our results show that the permeability and conductance increase dramatically by several orders of magnitude in peroxidized bilayers. Yet this increase is not sufficient to reasonably account for the entire range of experimental measurements. Nevertheless, lipid peroxidation might be considered an important mechanism of prolonged membrane permeabilization, if exposure of cells to high voltage electric pulses leads to secondary lipid peroxidation products. Our analysis calls for experimental studies, which will determine the type and amount of lipid peroxidation products in electropermeabilized cell membranes.

1. Introduction

Electroporation or electropermeabilization enables the control of cell membrane permeability by exposing cells to pulsed electric field [1]. This technique is nowadays applied in different biomedical and biotechnological fields, whether to gain access to the cytosolic compounds or for efficient delivery of exogenous molecules [2–6]. Nevertheless, the molecular mechanisms of electropermeabilization are still puzzling the researchers. It has become well-accepted that the increase in the transmembrane voltage induced by the electric field promotes formation of pores in the lipid bilayer. This has been argued by electrical and optical measurements on model lipid bilayers [7–10], theoretical analyses of the experimental results [11,12], and molecular dynamics (MD) simulations [13,14]. However, the electric-field-induced "electropores" do not seem to be able to explain all aspects of the electropermeabilization phenomenon. Specifically, the mechanisms of the sustained permeability of cell membranes, which persists long after pulse application, remain elusive. The complete resealing of the cell membrane takes several minutes at room temperature [15–17], which is about 8–9 orders of magnitude longer than the time of electropore closure as reported from MD investigations [18,19]. Experimental studies suggest that a possible alternative mechanism to explain the observed long-lived permeability of cell membranes is lipid peroxidation [20–32].

Lipid peroxidation refers to the oxidative degeneration of lipids, which is characterized by the formation of a hydroperoxide group in the lipid tails. The hydroperoxide group forms in a chain of reactions, which are initiated when a free radical attacks a weak allylic or bisallylic C—H bond [33,34]. During this chain of reactions, the intermediate peroxidation products propagate the radical damage to adjacent molecules, which means that a single free radial attack can lead to peroxidation of a patch of lipid molecules. The hydroperoxide lipid derivatives can ultimately reorganize and decompose into secondary products such as the cytotoxic 4-hydroxynonenal [35] and the mutagenic malondialdehyde [36]. The presence of oxidized lipids in a lipid membrane decreases the lipid order, lowers the phase transition temperature, leads to lateral expansion and thinning of the bilayer, alteration of bilayer hydration profiles, increased lipid mobility and augmented flip-flop, influences lateral phase organization and promotes formation

Abbreviations: CV, collective variable; d-AFED, driven adiabatic free energy dynamics; DLPC, dilinoleoyl-phosphatidylcholine; GUV, giant unilamellar vesicle; MD, molecular dynamics; PMF, potential of mean force; UFED, unified free energy dynamics.

* Corresponding authors.
E-mail addresses: l.rems@tudelft.nl; lea.rems@scilifelab.se (L. Rems), mounir.tarek@univ-lorraine.fr (M. Tarek).
[1] Present address: Department of Applied Physics, Science for Life Laboratory, KTH Royal Institute of Technology, 171 65 Solna, Sweden.

https://doi.org/10.1016/j.bioelechem.2018.07.018
1567-5394/

of water defects [37–39]. Therefore, oxidized bilayers are considerably more permeable and conductive than their non-oxidized counterparts.

The fact that electropermeabilization is accompanied by lipid peroxidation has been confirmed in bacteria [20,21], plant cells [22,23], and mammalian cells [23–25], as well as in liposomes made from polyunsaturated lipids [24–27]. Lipid peroxidation can be promoted by reactive oxygen species (ROS) already present in the solution before the delivery of electric pulses [26], although the exact mechanisms are not yet determined. Moreover, it has been shown that electric pulses can induce extracellular (electrochemical) [27,32] as well as intracellular [28–32] ROS generation. The latter is a consequence of the cellular response to the pulse treatment and can be detected specifically at the electropermeabilized part of the membrane [29]. Both ROS concentration and the extent of lipid peroxidation increase with electric field intensity, pulse duration, and number of pulses [23–31] and are correlated with cell membrane permeability and cell death [24,25,28–31]. An experimental study coupled with MD simulations further showed that oxidation of membrane components enhances the membrane susceptibility to electric-field mediated pore formation [40]. In addition, a theoretical study by Leguèbe et al. [41] suggested that lateral diffusion of peroxidized lipids along the membrane surface after each applied electric pulse could explain the influence of the pulse repetition frequency on electropermeabilization.

Nevertheless, the contribution of lipid peroxidation to the permeability of electropermeabilized cell membranes has not yet been quantitatively assessed. Indeed there are other possible mechanisms participating in the membrane permeability including changes in the conformation of membrane proteins [42–45]. To elucidate the role of lipid peroxidation in electropermeabilization such quantitative assessment needs to be carried out. This is a challenging task, which requires the characterization of the type and amount of lipid peroxidation products in electropermeabilized cell membranes, as well as the quantification of the permeability of the peroxidized parts of the membrane. In our study we make the first important step in this direction by quantifying the permeability and conductance of peroxidized bilayer patches to sodium and chloride ions using MD simulations and comparing our results against experimental measurements on electropermeabilized cells. The main idea which we follow in our study is schematically depicted in Fig. 1. We consider that exposure of a cell to electric pulses leads to formation of peroxidized lesions in the cell membrane. Such lesions can be formed in membrane domains rich in unsaturated lipids. These peroxidized lesions act as “hotspots” with high permeability and conductance, allowing locally enhanced transmembrane transport. To quantify the permeability and conductance of the lesions we resort to MD, as this allows us to study peroxidized bilayer patches with well-defined composition and investigate the underlying molecular mechanism of increased permeability. Since the types of lipid peroxidation products present in electropermeabilized cell membranes have not yet been well-characterized, we choose to study the polyunsaturated DLPC (1,2-dilinoleoyl-sn-glycero-3-phosphocholine) lipid molecule and its hydroperoxide derivatives. Peroxidized DLPC lipids can be considered as relevant models, since polyunsaturated lipids are the main targets of lipid peroxidation and since linoleic acid is one of the most abundant polyunsaturated fatty acids found in mammalian cells [46,47]. Finally, we use the calculated permeability and conductance to estimate the fraction of the cell membrane area which would need to be peroxidized to account for the increased ionic transport measured in electropermeabilized cell membranes after the pulse application. Our analysis allows us to draw conclusions whether peroxidized lesions could be sufficiently permeable to explain the long-lived post-pulse permeability of electropermeabilized cell membranes.

2. Methods

2.1. System preparation

The lipid bilayers were constructed by packing together replicas of a DLPC (1,2-dilinoleoyl-sn-glycero-3-phosphocholine) lipid molecule and/or its two main hydroperoxide derivatives (E,E-9-HPd and E,E-13-HPd, see Fig. 2) into a 64 molecules bilayer. Five different bilayer systems were prepared, with increasing percentage of peroxidized lipids, which we name 100% DLPC, 50% EE9, 50% EE13, 100% EE9, and 100% EE13. The bilayers were solvated with an aqueous 200 mM NaCl solution (~68 water molecules per lipid) (Table 1). The two bilayer systems with all lipids peroxidized (100% EE9 and 100% EE13) represent a part of a fully peroxidized cell membrane lesion. Such lesion could be formed as a consequence of the propagation of the oxidative damage from one lipid to its neighbouring lipids. Alternatively, such lesion could be formed by clustering of peroxidized lipids into local aggregates [48]. The two bilayer systems with 50% lipids peroxidized (50% EE9 and 50% EE13) represent a part of a peroxidized lesion which contains a homogeneous mixture of non-oxidized and peroxidized species. These systems are included in the study to test the influence of the concentration of peroxidized lipids on the bilayer permeability.

The non-oxidized DLPC molecules were described with the CHARMM36 force field [49–51]. The parameters required to describe the peroxidized group in the lipid tails were developed and described in a previous study [52]. The TIP3P model was used for water [53]. For Na and Cl ions we took the Lennard-Jones parameters from CHARMM36 force field. However, in assigning their charges we followed recent studies, which demonstrated that rescaling ionic charges by the inverse square root of the electronic part of the solvent dielectric constant (a factor of 0.75 for water) leads to important improvements in the description of electrolyte solutions [54–56]. Such rescaling, termed the electronic continuum correction, effectively takes into account the electronic polarization effect of the solvent, which is missing in typical non-polarizable MD simulations. Note that we observed better agreement between the calculated bilayer permeability and experimental results after rescaling the charges of Na and Cl, as described in Supplementary Section S4.

Finally, it should be noted that our study focuses exclusively on the permeability of an electropermeabilized cell membrane which persists

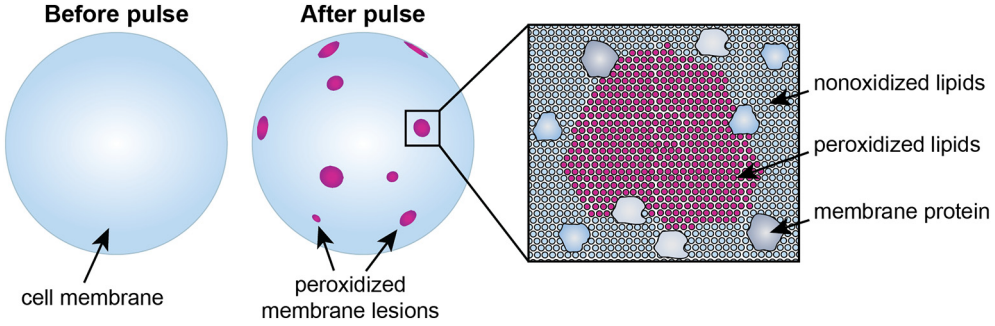

Fig. 1. Schematic representation of peroxidized membrane lesions, which are expected to be formed in the cell membrane after exposure to electric pulses. The schematic is hypothetical and the lesions are not drawn to scale. The image on the right schematically depicts the molecular organization in one of the lesions.

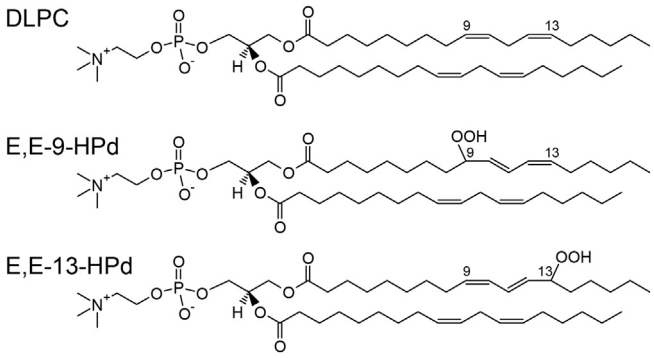

Fig. 2. Structure of the lipid molecules considered in this work.

long after pulse application, when the cell is no longer exposed to an external electric field. Therefore, all simulations were carried out in the absence of an electric field.

2.2. System equilibration

All simulations were performed in GROMACS 4.6.4 [57]. Each system was first minimized using the steepest descent algorithm for energy minimization. The equilibration was then carried out in the NpT ensemble (constant number of molecules N, pressure p and temperature T) using the Berendsen [58] thermostat ($\tau = 0.1$ ps) and barostat ($\tau = 2.0$ ps, semi-isotropic coupling) for 5 ns at $T = 300$ K and $p = 50$ bar, followed by 5 ns at $T = 300$ K and $p = 1$ bar. In this initial part, the equations of motion were integrated using the leap-frog integrator with a time step of 1.0 fs. Afterwards, the equilibration was continued in the NpT ensemble at $T = 300$ K and $p = 1$ bar using the Nose-Hoover thermostat ($\tau = 1.6$ ps) [59,60] and Parrinello-Rahman barostat ($\tau = 2.0$ ps, semi-isotropic coupling) [61,62]. This second part of the equilibration was carried out for at least 300 ns using the leap-frog integrator with a time step of 2.0 fs. The long-range electrostatic interactions were calculated using Particle Mesh Ewald method [63] together with a Fourier grid spacing of 0.16 nm and a cutoff of 1.2 nm. A switching function was used between 0.8 and 1.2 nm to smoothly bring the short-range electrostatic interactions and the van der Waals interactions to 0 at 1.2 nm. The chemical bonds between hydrogen and heavy atoms were constrained to their equilibrium values using the LINCS algorithm [64]. Periodic boundary conditions were applied in all directions.

To verify the convergence of the equilibration we monitored the time course of the bilayer thickness, area per lipid, and the number of hydrogen bonds between the OOH groups and water or lipid oxygen atoms [65]. The bilayer thickness was defined as the distance between the centres of mass of phosphate atoms in each of the bilayer leaflet. The area per lipid was determined as the area of the simulation box in the (x, y)-plane divided by the number of lipids in one leaflet. The number of hydrogen bonds was extracted using the VMD [66] function *measure hbonds*, using a cutoff distance of 0.35 nm and cutoff angle of 30°.

The electrostatic potential profiles along the membrane normal were derived from MD simulations using Poisson's equation and expressed as the double integral of the molecular charge density distribution $\rho(z)$:

$$\Phi(z) = -\varepsilon_0^{-1} \iint \rho(z'')\mathrm{d}z''\mathrm{d}z' \tag{1}$$

z being the position of the charge in the direction along the normal to the bilayer.

Note that the systems were first equilibrated considering the full charge of the Na and Cl ions. During the last ~100 ns of the equilibration, the ionic charge was rescaled by a factor of 0.75 (Section 2.1). No considerable difference in the membrane thickness, area per lipid, number of hydrogen bonds, or the dipole potential was found when using the full or rescaled charge (Supplementary Fig. S1). However, the binding of Na ions to lipid headgroups was reduced after rescaling the charge (Supplementary Fig. S2).

Table 1
The number of molecules and the size of the simulation box in the investigated bilayer systems.

System	DLPC	E,E-9-; HPd	E,E-13-; HPd	water	Na	Cl	Simulation box size
100% DLPC	64	0	0	4361	17	17	$4.5 \times 4.5 \times 10.6$ nm^3
50% EE9	32	32	0	4311	17	17	$4.7 \times 4.7 \times 9.5$ nm^3
50% EE13	32	0	32	4357	17	17	$4.7 \times 4.7 \times 9.4$ nm^3
100% EE9	0	64	0	4325	17	17	$4.8 \times 4.8 \times 9.0$ nm^3
100% EE13	0	0	64	4344	17	17	$4.9 \times 4.9 \times 8.7$ nm^3

2.3. Potential of mean force (PMF) profiles

Classical MD simulations are not suited to explore rare events such as permeation of an ion across the bilayer. It is therefore necessary to resort to specific techniques, known as "free energy" methods, which allow one to calculate the free energy profile along a chosen collective variable (CV). A CV maps the atomic coordinates onto a low-dimensional space in which relevant conformations of the system are well separated. In this study we used the recently developed method Unified Free Energy Dynamics (UFED) [67,68] to obtain the potential of mean force (PMF) profiles of an ion along the position normal to the bilayer plane. The UFED method combines the ideas from the driven Adiabatic Free Energy Dynamics (d-AFED, also known as Temperature Accelerated Molecular Dynamics) [69,70] and Metadynamics [71,72], resulting in superior convergence properties with respect to both original methods [68]. The principle of d-AFED is based on connecting a CV with a harmonic potential to an extended variable (an imaginary particle), which is adiabatically decoupled from the physical system. This allows the extended variable to be kept at temperature T_s, which is higher than the temperature of the physical system T. The temperature T_s is typically set such that the energy $k_B T_s$ (where k_B is the Boltzmann constant) is comparable to the height of the free energy barriers in the phase space of the CV. The extended variable can therefore easily cross the energy barriers, dragging along the CV, which results in enhanced sampling of the relevant configurations within the physical system. In UFED, an additional history-dependent bias potential is added to the extended variable to penalize the regions already sampled, which makes the sampling of the phase space more homogeneous. The bias potential is similar to the one used in Metadynamics and is in the form of Gaussians (hills) with height h and width σ, which are gradually deposited along the extended variable trajectory. If the adiabatic separation is effective, the PMF $\phi(s)$ can be recovered from the force $F(s)$ on the extended variable by a posteriori numerical integration [67,68]

$$\begin{aligned} F(s) &= -\frac{\partial \phi(s)}{\partial s} = \kappa(q - s)_s \\ \phi(s) &= -\int_{s_{min}}^{s_{max}} F(s)\mathrm{d}s \end{aligned} \tag{2}$$

where s and q denote the extended variable and the collective variable, respectively, and κ denotes the coupling constant of the harmonic potential between the extended and physical space. The adiabatic decoupling is achieved by choosing a large κ and by assigning large mass m_s to the extended variable.

2.3.1. UFED parameters

Although UFED allows multiple CVs to be explored simultaneously, we were primarily interested in the PMF of an ion along the direction normal to the bilayer plane (z-axis). Therefore, we defined the CV as the z-position of a chosen ion. To prevent movement of the bilayer in

the z-direction, the centre of mass of all phosphorus atoms was constrained at a fixed z-position using a harmonic potential with a spring constant of 3500 kJ/mol/nm^2. This was done in PLUMED using the directive "UMBRELLA". The chosen spring constant resulted in fluctuations of the centre of mass of the phosphorus atoms with a standard deviation of ~0.01 nm.

The UFED parameters consist of the d-AFED parameters (κ, m_s, T_s) and the parameters of the bias potential (h, σ, and the hill deposition rate). The chosen values of the UFED parameters are summarized in Table 2 and explained in the Supplementary Section S2.1.

2.3.2. UFED simulation protocol

All UFED simulations were performed with GROMACS 4.6.3 patched with PLUMED 1.3 software [73] including the code to perform d-AFED/UFED free-energy calculations [74]. The simulations parameters for the physical system were the same as during equilibration (Section 2.2), except that the simulations were performed in the NVT ensemble (constant number of molecules N, volume V and temperature T; the used PLUMED version does not enable simulations in the NpT ensemble). Moreover, in these simulations the biased ion was coupled to a Nose-Hoover thermostat ($\tau = 1.6$ ps) separately from other atoms in the system.

To increase the efficiency of the exploration of the phase space, each UFED simulation was performed by running 8 walkers in parallel. Each walker started at a different initial configuration. These initial configurations were obtained by steering the studied ion from the bulk towards the centre of the bilayer with a steering velocity of 0.25 nm/ns and a spring constant of 3500 kJ/mol/nm^2 using PLUMED directive "STEER". The UFED simulation was carried out for at least 80 ns per walker. If the PMF profile did not appear converged by then, the simulation was prolonged to 120 ns. Representative trajectories of individual walkers within a UFED simulation run are shown in Supplementary Fig. S4. The output for the UFED variables (q, s, etc.) was saved every 0.04 ps.

2.3.3. Analysis of the PMF profiles

The PMF profile was determined according to Eq. (2) using custom Matlab scripts (Matlab R2017a, MathWorks), which were adapted from the scripts developed by M. A. Cuendet [68]. The interval $z = [-3.0, 0.0]$ nm was divided into 120 bins, and the force $F = \kappa(q - s)$, sampled over the UFED run, was binned and averaged within each bin. The force was then slightly smoothed with a kernel smoothing regression (Matlab function ksr) with bandwidth of 1/30 nm. Finally, the force was integrated with cumulative trapezoidal numerical integration (Matlab function cumtrapz) to obtain the PMF over the interval $z = [-3.0, 0.0]$ nm. This profile was then mirrored across the centre of the bilayer ($z = 0.0$ nm).

To ensure that a PMF profile was converged and to estimate the uncertainty of the profile we performed an additional UFED run for each of the investigated systems. This second UFED run was performed in the same way as the first run, except that the initial configurations of the walkers were different. The PMF profiles were determined for the first and the second UFED run separately, as well as for both UFED runs together. The latter is presented in the manuscript as the final PMF profile, whereas the minimum and maximum value obtained at a given z-position in the two individual runs are presented as the error bars. Comparison between the PMF profiles obtained with the two UFED runs was also used to confirm the convergence of each PMF profile (Supplementary Section S2.3).

Table 2
The values of the UFED parameters.

Parameter	Symbol	Value
Coupling constant	κ	$1 \cdot 10^5$ kJ/mol/nm^2
Mass of the extended variable	m_s	$2 \cdot 10^4$ amu
Temperature of the extended variable	T_s	400 K
Hill height	h	1.0 kJ/mol
Hill width	σ	0.01 nm
Hill deposition rate		0.1 ps^{-1}

2.4. Diffusion coefficients

The diffusion coefficients (in m^2/s) were determined similarly as in [75]. An ion was constrained at different z-positions using a harmonic potential with a spring constant of 3500 kJ/mol/nm^2 (PLUMED's directive "UMBRELLA"). No constrain was imposed on x and y positions. The initial configurations were taken from the simulation when the ion was steered to the centre of the bilayer (positions from −3.0 nm to 0 nm, separated by 0.1 nm). Other simulation parameters were the same as in UFED simulations. For each position, a 5-ns-long trajectory was obtained, where the first ns was considered as equilibration. The remaining 4-ns-long trajectory was divided into four parts. For each of the four parts the diffusion coefficient at i-th position was calculated as

$$D_i = \frac{\left\langle \delta z^2 \right\rangle_i}{\tau_i} \tag{3}$$

The variable τ_i is the correlation time at i-th position and was calculated following the method of Hummer [76] (see also the Supporting material in [75])

$$\tau_i = \lim_{s\to 0} \tau_i(s) = \lim_{s\to 0} \frac{\hat{C}_z(s; z_i)}{\left\langle \delta z^2 \right\rangle_i} = \lim_{s\to 0} \frac{\int_0^\infty e^{-st} \langle \delta z(t) \delta z(0) \rangle_i \mathrm{d}t}{\left\langle \delta z^2 \right\rangle_i} \tag{4}$$

where s is the inverse time, $\delta z = z - \langle z \rangle_i$ is the position displacement, and $\hat{C}_z(s; z_i)$ is the Laplace transform of the position autocorrelation function. The values of $\tau_i(s)$ were calculated at $s = 0.05, 0.1, 0.2, \ldots, 1.0, 2.0, \ldots, 10, 20$ ps^{-1}. $\tau_i(s)$ were extrapolated to $s = 0$ by fitting the function $a/(s + b)$ [75]. In some instances, the fitting was performed from $s = 0.1$ ps^{-1} or larger due to oscillatory behaviour of the autocorrelation function and consequently $\tau_i(s)$. D_i obtained from each of the four 1-ns-long parts of the trajectory was averaged. The averages values were finally smoothed with a kernel smoothing regression (Matlab function ksr) with bandwidth of 0.2 nm. The smoothed profile was used in the calculation of membrane permeability.

2.5. Calculation of membrane permeability and conductance

The bilayer permeability (in m/s) was calculated according to an inhomogeneous solubility-diffusion model [75,77].

$$P_{ion} = \left(\int_{z_1}^{z_2} \frac{\exp(\phi_{ion}(z)/RT)}{D_{ion}(z)} \, dz \right)^{-1} \tag{5}$$

where $\phi_{ion}(z)$ is the single ion PMF along the z-axis (in kJ/mol), R is the universal gas constant, T the temperature and $D_{ion}(z)$ the diffusion coefficient of the ion along the z-axis. The integration boundaries were taken as $z = [-3.0, 3.0]$ nm. The calculations of $\phi_{ion}(z)$ and $D_{ion}(z)$ are explained in Sections 2.3 and 2.4, respectively. The uncertainty in the calculated P_{ion} was estimated in the following way. First, the permeability was determined using PMFs from trajectories of each of the two UFED runs and from trajectories of both runs together. The latter was considered as the mean value, whereas the former two were used to determine the lower and upper value of P_{ion}. In addition, this lower and upper value of P_{ion} was further multiplied by a factor of 0.5 and 1.5, respectively, to take into account the estimated 50% uncertainty in the calculated $D_{ion}(z)$ (the estimation of the uncertainty in $D_{ion}(z)$ is explained in Supplementary Section S3).

The membrane conductance (in S/m^2) for NaCl was calculated as [75,78].

$$G_m = G_{Na} + G_{Cl} = \frac{N_A {q_e}^2}{k_B T} c(P_{Na} + P_{Cl}) \quad (6)$$

where G_{Na} and G_{Cl} are contributions of Na and Cl ions, respectively, to the total membrane conductance and can be calculated via

$$G_{ion} = \frac{N_A {q_e}^2}{k_B T} c P_{ion} \quad (7)$$

The constants N_A, q_e, k_B are, respectively, the Avogadro constant, the elementary charge, and the Boltzmann constant, $T = 300$ K is the temperature and $c \approx 200$ mM is the bulk concentration of NaCl. The uncertainty of G_m was determined based on the uncertainty of P_{Na} and P_{Cl}:

$$u(G_m) = \frac{N_A {q_e}^2}{k_B T} c \sqrt{u^2(P_{Na}) + u^2(P_{Cl})} \quad (8)$$

3. Results

3.1. Properties of equilibrated peroxidized bilayers

The presence of the peroxide groups in the lipid tails influences the bilayer properties. Fig. 3 shows the molecular configuration of bilayers with increasing percentage of peroxidized lipids. The non-oxidized 100% DLPC bilayer has a thickness of 3.92 ± 0.08 nm (defined as the distance between the centres of mass of phosphate atoms). This is within 10% of the experimental value of 3.6 nm obtained from X-ray scattering at 5 °C [79]. The area per lipid of pure DLPC bilayer is 0.64 ± 0.02 nm^2, which is close to the area per lipid obtained on a similar PLPC (1-palmitoyl-2-linoleoyl-sn-glycero-3-phosphatidylcholine) bilayer using MD, i.e., 0.651 ± 0.015 nm^2 [38]. The thickness and area per lipid decrease and increase, respectively, with increasing percentage of peroxidized lipids (Fig. 4a), which is in agreement with previous MD simulations and experiments [38,79]. The peroxidized bilayers exhibit a decrease in the dipole potential as well (Fig. 4b). Note that the dipole potential peak maxima in the centre of the bilayer is compatible with experimental findings from CryoEM measurements [80].

The EE9 and EE13 hydroperoxide derivatives differ in the position of the polar OOH group in the carbon chain. The OOH group is positioned at the 9th and 13th carbon in EE9 and EE13 lipid, respectively. Due to this different position, the distribution of the OOH groups in EE9 and EE13 bilayers differs markedly. In EE9 bilayers, the OOH groups on average prefer to reside next to the head-group region, as can be seen from the density profiles in Fig. 5a and Fig. 5c. In EE13 bilayers, the density profile of OOH groups exhibits peaks both at the head-group region and in the middle of the bilayer (Fig. 5b and Fig. 5d). In the 100% EE13 bilayer the highest density of OOH groups is found in the middle of the bilayer. This already suggests that EE13 bilayers can provide a more favourable environment for ion permeation.

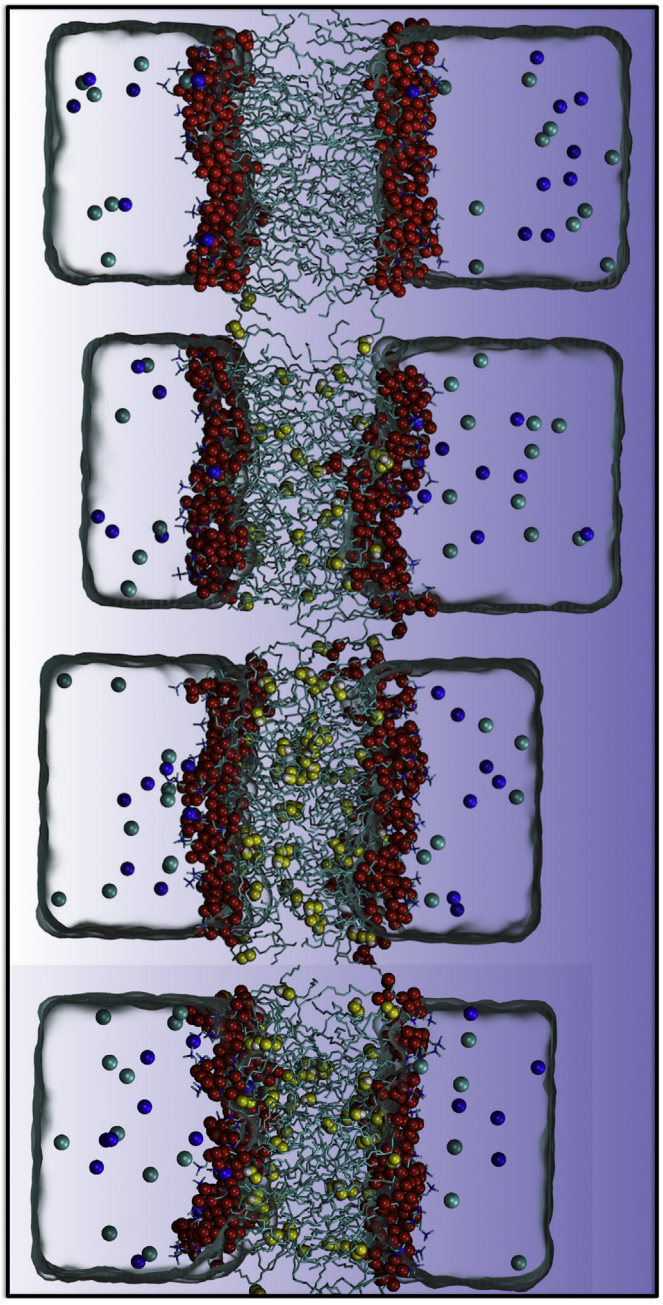

Fig. 3. Molecular configuration of systems with increasing percentage of peroxidized lipids. From left to right: 100% DLPC, 50% EE13, 100% EE13, and 100% EE9. The lipids are represented with cyan bonds and the P and N atoms are shown as red spheres. Water is shown as transparent surface, Na and Cl ions are shown as blue and cyan spheres, respectively. The O and H atoms of the OOH groups are shown as yellow and white spheres, respectively. (For interpretation of the references to color in this figure legend, the reader is referred to the web version of this article.)

3.2. Potential of mean force (PMF) profiles

The PMF profiles of Na and Cl ion in the investigated bilayer systems are shown in Fig. 6. All profiles are Λ-shaped, consistent with the profiles obtained in different non-oxidized bilayers in previous studies [75,81]. With increasing percentage of peroxidized lipids, the height of the profile progressively decreases both for Na and Cl ion. The bilayers with the hydroperoxide derivative EE13 exhibit lower PMF profiles than EE9 at the same percentage of peroxidized lipids. The height of the PMF profile reduces in peroxidized bilayers, since the polar peroxide groups can participate in hydrating the ion within the bilayer (Fig. 5). In addition, the reduction of the PMF profile can be attributed to the smaller membrane thickness, larger area per lipid, and to some extent a lower dipole potential of peroxidized bilayers (Fig. 4).

3.3. Bilayer permeability and conductance

By knowing the PMF profile and the diffusion coefficient profile of the ions it is possible to calculate the bilayer permeability to a given ion using Eq. (5). The diffusion coefficient profiles are similar for all investigated systems and are shown in Supplementary Fig. S6. Inside the bilayer, the diffusion coefficient of an ion reduces by about an order of magnitude with respect to its bulk value. Knowing the bilayer

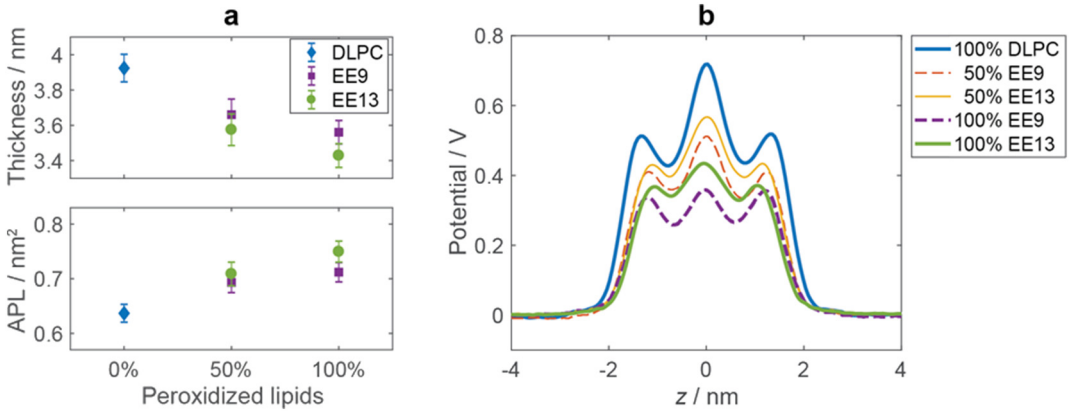

Fig. 4. The thickness, area per lipid (APL), and electric potential of the investigated bilayer systems. The electric potential is shown along the axis normal to the bilayer plane. The centre of the bilayer is at $z = 0$ nm.

permeability for Na and Cl, we can also calculate the membrane conductance in NaCl solution using Eq. (6). The calculated values are presented in Fig. 7 together with the experimentally measured permeability and conductance on various non-oxidized bilayers. Firstly, by comparing the calculated values in 100% DLPC (0% peroxidized lipids) with experimental data we find good agreement. There is large spread of experimental data for the permeability to Cl, whereby our calculations agree well with the lower measured values. Secondly, it can be seen that the permeability and conductance increase dramatically with increasing percentage of peroxidized lipids. The permeability for Na increases by 4–5 orders of magnitude in bilayers with 50% peroxidized lipids: i.e. from $4.8 \cdot 10^{-16}$ m/s in 100% DLPC bilayer to $1.8 \cdot 10^{-12}$ and $1.2 \cdot 10^{-11}$ m/s in 50% EE9 and 50% EE13 bilayers, respectively. The increase is even greater in bilayers with 100% peroxidized lipids reaching $0.8 \cdot 10^{-10}$ and $2.0 \cdot 10^{-8}$ m/s in 100% EE9 and 100% EE13 bilayers, respectively. Similar can be observed in the permeability for Cl. The permeability for Cl increases from $1.2 \cdot 10^{-13}$ m/s in 100% DLPC bilayer to $0.7 \cdot 10^{-11}$, $2.4 \cdot 10^{-10}$, $3.0 \cdot 10^{-10}$, and $1.5 \cdot 10^{-8}$ m/s in 50% EE9, 50% EE13, 100% EE9, and 100% EE13 bilayers, respectively. Note that the highest increase, 8 orders of magnitude for Na and 5 orders of magnitude for Cl, is found in 100% EE13 bilayer. The increase in permeability is reflected also in increased membrane conductance. The highest value of 26 S/m^2 is calculated in 100% EE13 bilayer, which corresponds to an increase of 5 orders of magnitude with respect to the conductance of the non-oxidized 100% DLPC bilayer.

4. Discussion

Experimental studies suggest that lipid peroxidation could present a mechanism of the long-lived cell membrane permeability, which persists for minutes after exposing the cells to electric pulses [20–32]. The aim of our study is to investigate whether peroxidized lesions in the cell membrane could be permeable enough to account for the post-pulse membrane permeability and conductance measured in electropermeabilized cells. Therefore, we calculated the permeability and conductance of lipid bilayer patches containing hydroperoxide lipid derivatives using free energy calculations in MD. The next step that we need to do to quantify the possible role of lipid peroxidation in electropermeabilization is to use the calculated values and compare them to experimental measurements on electropermeabilized cells. Unfortunately, the permeability and conductance of the cell membrane are seldom quantified in electropermeabilization studies. Below we use available experimental results from four research groups, which measured either the membrane permeability or conductance after exposure of cells to electric pulses. However, the comparison between our results from MD and experimental measurements requires some intermediate

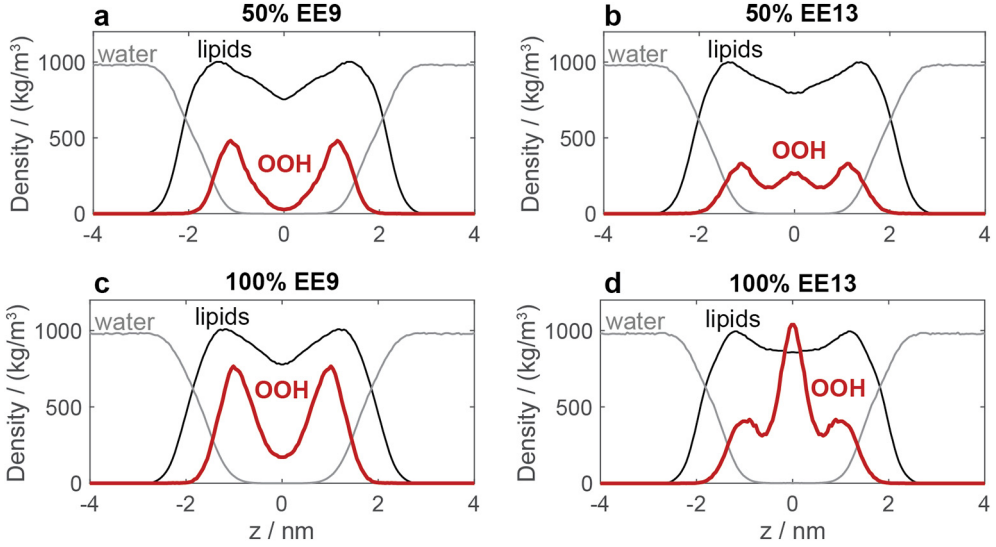

Fig. 5. Density profiles along the axis normal to the bilayer plane showing the preferred location of the OOH groups. For each bilayer system the density profile is shown for lipids (thin black line), water (thin grey line) and OOH groups (thick red line).The density of OOH groups was scaled by a factor of 10. (For interpretation of the references to color in this figure legend, the reader is referred to the web version of this article.)

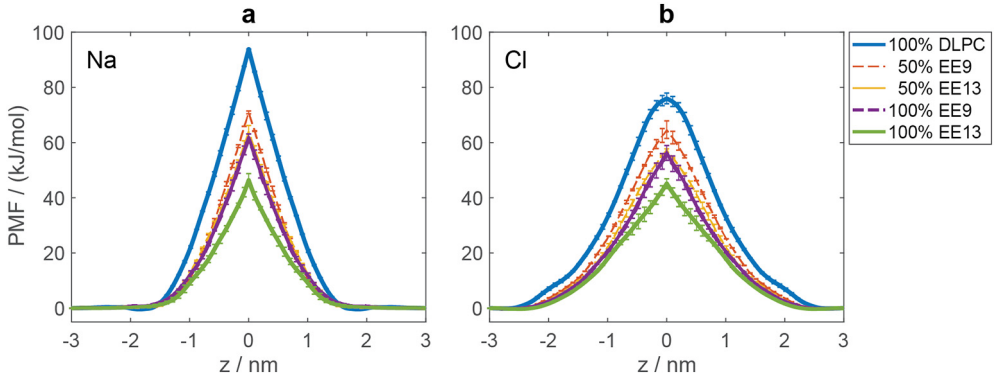

Fig. 6. The PMF profiles of Na ion (a) and Cl ion (b) in the investigated bilayer systems. The centre of the bilayer is at $z = 0$ nm.

steps. Experimental measurements are carried out over the entire cell membrane surface, whereas the bilayer systems investigated in MD are representative of a small part of a peroxidized lesion. If the area of peroxidized lesions in electropermeabilized cell membranes was known, we could calculate the total ionic transport through the lesions and compare it directly to the measurements. This would allow us to estimate the fraction of the ionic transport that can be attributed to lipid peroxidation. However, the area of the lesions is at present unknown. Therefore, we instead estimate the fraction of the cell membrane that would need to be peroxidized to account for the experimental measurements. We carry out these estimates under the hypothesis that the transport of ions across electropermeabilized cell membranes takes place mainly through peroxidized membrane lesions. The estimates then give an insight whether lipid peroxidation could play the role of the dominant or merely a participating mechanism in the long-lived permeability of electropermeabilized cell membranes.

4.1. Comparison with experimental measurements of the permeability of electropermeabilized cell membranes

Shirakashi et al. [87] estimated the membrane permeability of mouse myeloma (Sp2) cells to KCl and trehalose by monitoring the changes in the cell volume due to osmotic shrinkage after electropermeabilization. They delivered a single 20 μs pulse resulting in 2–3 kV/cm. Under these conditions ≥80% cells survived the pulsing. The estimated permeability was actually an effective permeability P_{eff} averaged over the entire membrane surface and corresponded to the expression

$$\frac{dn_i}{dt} = P_{eff}\,\exp\left(-\frac{t}{\tau}\right)(c_e - c_i)A_{cell} \tag{9}$$

where n_i is the number of moles of a given ion inside the cell, c_e and c_i are the extracellular and intracellular ionic concentration, respectively, and A_{cell} is the cell membrane area. The permeability was assumed to decrease after the pulse with a time constant τ between 191 s and 289 s, consistent with their experimental findings. The estimated P_{eff} to KCl was between ~$4 \cdot 10^{-9}$ m/s and ~$22 \cdot 10^{-9}$ m/s.

We now revisit their results under the assumption that in an electropermeabilized membrane most of the ions cross the membrane across peroxidized lesions. Hence, we write

$$\frac{dn_i}{dt} = P_{ox}(c_e - c_i)A_{ox} \tag{10}$$

where P_{ox} and A_{ox} are the permeability and total area of the peroxidized lesions, respectively. By comparing Eqs. (9) and (10) we find the areal fraction of peroxidized lesions f_{ox} at the beginning of the membrane resealing phase:

$$f_{ox} = \frac{A_{ox}}{A_{cell}} = \frac{P_{eff}}{P_{ox}} \tag{11}$$

Knowing the permeability of peroxidized bilayer lesions P_{ox}, we can estimate how much of the cell membrane area should be peroxidized to yield the P_{eff} values estimated by Shirakashi et al. [87]. For P_{ox} we use our highest calculated permeability value of $2.0 \cdot 10^{-8}$ m/s (Na in 100% EE13 bilayer). Although there are known differences between Na and K interactions with non-oxidized bilayers [88,89], we expect that in 100% peroxidized bilayers the permeabilities for K, Na, and Cl ions are similar, since we observed practically no difference between the permeabilities for Na and Cl ions (Fig. 7).The corresponding estimated peroxidized area is between about 20% and 110% of the cell membrane.

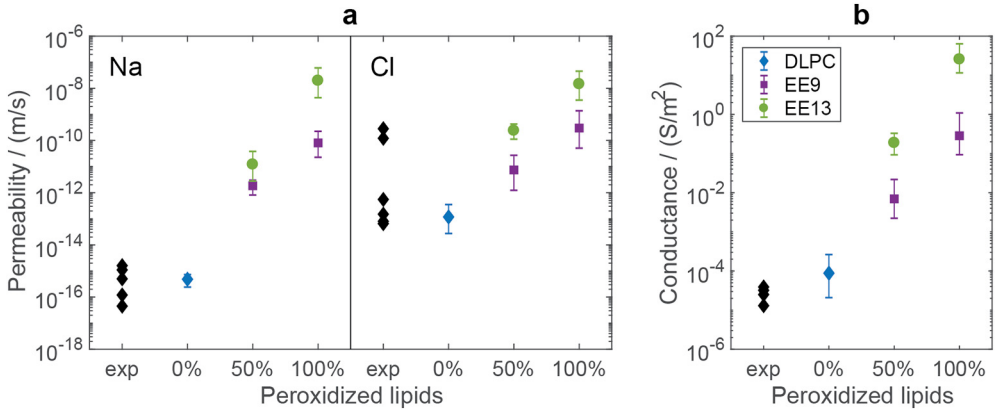

Fig. 7. Permeability and conductance of bilayers with increasing percentage of peroxidized lipids. Black diamonds (exp) show experimental measurements of the permeability to Na and Cl and the conductance in NaCl solutions, performed on different non-oxidized lipid bilayers. The experimental values for permeability were taken from [75,82–85], and the experimental values for conductance from [75,86]. Further details on the experimental values are given in Supplementary Tables S2 and S3.

The predicted range of peroxidized area is unreasonable, since only a fraction of the cell surface is covered by lipids (membrane proteins constitute roughly 50% of the cell membrane weight [90]) of which not all of the lipids are unsaturated and oxidizable. This suggests that the permeability of peroxidized lipids is too low to account for the entire range of measurements, meaning that peroxidized lesions cannot be the only mechanism of ionic transport under the given experimental conditions.

Pavlin et al. [91,92] studied the changes in conductivity of dense cell suspensions during and in between the delivery of multiple electric pulses. Mouse melanoma (B16-F1) cells were exposed to eight 100 μs, 1 kV/cm pulses, with a repetition frequency of 1 Hz. Under these conditions, the cell viability was ~90% [93]. They observed that in between consecutive pulses the conductivity of the suspension increases due to the leak-out of cytosolic ions into the extracellular medium. Given that the extracellular medium lacked K^+ ions, the leak-out was primarily attributed to K^+ ions. The characteristic time in which the suspension conductivity increased after each pulse was described as

$$\frac{dn_e}{dt} = -(c_e - c_i)\frac{Df_{per}}{d}A_{cell,tot} \tag{12a}$$

The ions were assumed to flow through long-lived pores, where f_{per} is the areal fraction of the pores in the cell membrane, D is an effective diffusion coefficient of an ion inside a pore, $d = 5$ nm is the cell membrane thickness, and $A_{cell,tot}$ is the membrane area of all cells in the suspension. Note that Eq. (12a) corrects a typo in the original paper and replaces the membrane area of a single cell with $A_{cell,tot}$. Eq. (12a) can be rewritten in terms of the characteristic time τ in which the suspension conductivity increases after each pulse

$$\frac{dn_e}{dt} = -(c_e - c_i)\frac{(1-F)R}{3\tau}A_{cell,tot} \tag{12b}$$

where $R = 8.5$ μm is the cell radius and $F = 0.3$ is the volume fraction of cells [92]. The measured characteristic time decreased with each subsequent pulse from 34.5 s after the first pulse to 9.1 s after the seventh pulse [92].

Assuming that the ions do not flow through pores but rather through peroxidized lesions, we can write an analogous expression

$$\frac{dn_e}{dt} = -P_{ox}(c_e - c_i)A_{ox,tot} \tag{13}$$

By comparing Eqs. (12b) and (13) we again find the expression for f_{ox}

$$f_{ox} = \frac{A_{ox,tot}}{A_{cell,tot}} = \frac{(1-F)R/(3\tau)}{P_{ox}} \tag{14}$$

where $P_{eff} = (1 - F)R/(3\tau)$ is analogous to the effective permeability measured by Shirakashi et al. [87]. For τ between 34.5 s and 9.1 s the peroxidized fraction f_{ox} would need to be between about 290% and 1090%, which is unreasonable. The results of Pavlin et al. [91,92] suggest higher membrane permeability P_{eff} than the results of Shirakashi et al. [87]. This is possibly because the permeability estimated by Pavlin et al. corresponds to the permeability within the first second after the pulse, whereas Shirakashi et al. monitored the permeability over minutes after the pulse.

In summary, both the measurements of Shirakashi et al. [87] and Pavlin et al. [91,92] suggest that the permeability of peroxidized bilayers calculated in our study is too low to reasonably account for the experimentally observed ionic transport. Nevertheless, since the experiments involved volumetric cell changes (cell shrinkage in [87] and cell swelling in [91,92]), it is possible that part of the ionic transport was mediated by opening of K channels in the membrane [96]. It should also be noted that both Shirakashi et al. and Pavlin et al. analysed their data using many simplifying assumptions, which raises some doubt in the accuracy of the reported values of the permeability and ionic flux.

4.2. Comparison with experimental measurements of the conductance of electropermeabilized cell membranes

We further compare our calculations on peroxidized bilayers with experimental measurements of the conductance of electropermeabilized cell membranes. Wegner et al. [45] studied the changes in the membrane conductance in Chinese hamster lung fibroblasts (DC-3F cells) using whole-cell patch clamp. The patch-clamp setup was used to both increase the transmembrane voltage above the electroporation threshold and measure the membrane conductance during and after application of a porating electric pulse. The electroporation pulses were 5–10 ms long. They observed that conductance changes can be separated into two distinct modes. The first mode, termed transient electroporation, appeared during the pulse when the membrane conductance increased 8–100×. After the pulse this increase exponentially declined with a time constant of ~17 ms. This transient electroporation mode could be due to opening of membrane pores, which collapse/close on the millisecond time scale after the pulse [9]. The second mode, termed persistent permeabilization, corresponded to the state in which the membrane conductance remained slightly elevated for at least 40 min after the pulse. This mode was observed only when applying a pulse with considerably higher amplitude than the one required to trigger transient electroporation, or when applying multiple pulses. The membrane conductance in the state of persistent permeabilization ranged from 0.088 to 3.3 nS/pF [45].

Pakhomov et al. [97,98] also studied the changes in membrane conductance using whole-cell patch clamp. However, they performed their measurements after exposing the cells to short nanosecond pulses delivered by a pair of wire electrodes. When exposing GH3 cells (rat pituitary tumor cells) to one and five pulses of 60 ns, 12 kV/cm, the membrane conductance increased by ~0.05 nS/pF and ~0.5 nS/pF, respectively, compared to control. These measurements were carried out about 2 min after pulsing; however, the recovery of the conductance took >10 min. In a follow-up study [99] they were able to measure the conductance in shorter time after the pulse (5 to 10 s). They compared the conductance of individual GH3 cells before and after the pulse. When exposing cells to a single 60 ns pulse with amplitude in the range of 4.8–14.6 kV/cm, the conductance increased in the range of 0.1–1.5 nS/pF (these values were obtained by normalizing the values from their Fig. 3a [99] with the capacitance of GH3 cells of 6 pF [98]). When applying multiple pulses, the measured increase in conductance could go up to 5.7 nS/pF [99]. Note that the range of values measured by Pakhomov et al. [97–99] is similar to the range measured by Wegner et al. [45] in the persistent permeabilization mode.

Similarly as above, we can estimate the fraction of the cell membrane that would need to be peroxidized to explain the experimentally measured increase in cell membrane conductance Δg (in units nS/pF)

$$f_{ox} = \frac{A_{ox}}{A_{cell}} = \frac{\Delta g C_m}{G_{ox}} \tag{15}$$

where C_m is the capacitance per unit of cell membrane area (~1 μF/cm^2 [100,101]) and G_{ox} is the conductance of a peroxidized bilayer lesion. For G_{ox} we take the highest value of 26 S/m^2 obtained in 100% EE13 bilayer. Fig. 8 shows some of the measured change in membrane conductance Δg and the corresponding estimated f_{ox}. For the smallest values of Δg, the predicted fraction of peroxidized lipids is on the order of 1%. However, larger values of Δg would require the entire cell membrane to be peroxidized.

In summary, our comparison between the calculated conductance of peroxidized bilayers and experimental measurements suggests that lipid peroxidation could have a measurable effect on the membrane conductance, equal to the lowest measured values in electropermeabilized

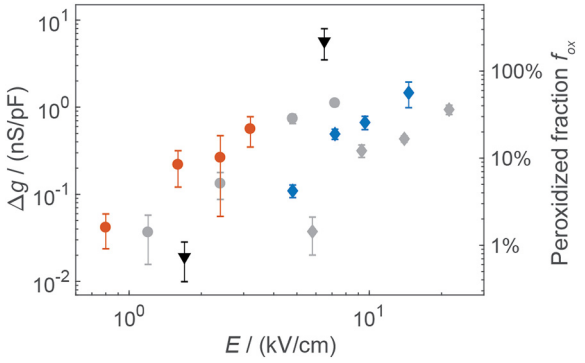

Fig. 8. Increase in membrane conductance measured in GH3 cells after exposure to nanosecond electric pulses. The scale on the right side shows the corresponding estimated fraction of peroxidized membrane lesions. The experimental values of Δg were taken from studies of Ibey et al. [99,103] The values of the membrane resistance reported in [103] were inverted and normalized to the capacitance of GH3 cells of 6 pF [98]. Grey symbols show measurements conducted 2–3 min after pulsing [103]. Colored symbols show measurements conducted 5–10 s after pulsing [99]. Grey and blue diamonds = single 60 ns pulse; grey circles = single 600 ns pulse; red circles = hundred 60 ns pulses. Black triangles show the minimum and maximum value measured when using various parameters of nanosecond pulses [99]. (For interpretation of the references to color in this figure legend, the reader is referred to the web version of this article.)

cells, even if only 1% of the cell membrane was peroxidized. However, the conductance of peroxidized bilayers calculated in our study is too low to account for the entire range of experimental values. The possibility that part of the experimentally measured conductance was mediated by ion channels, which were (de)activated or modified due to electric field exposure, cannot be completely excluded [94,102]. Nevertheless, it is unlikely that ion channels were the dominant conduction pathway, since similar change in conductance was observed in GH3 and CHO cells, whereby CHO cells express very few endogenous ion channels [103].

4.3. Secondary lipid peroxidation products and spontaneous pore formation in oxidatively damaged membrane lesions

The discussion in Sections 4.1 and 4.2 indicates that the permeability and conductance of peroxidized lipids are not sufficiently high to reasonably account for the entire range of experimental measurements of ionic transport in electropermeabilized cells. However, it should be kept in mind that our analysis is based on hydroperoxide lipid derivatives, which correspond to the primary peroxidation products. Though lipid hydroperoxides are stable enough to persist and diffuse in lipid bilayers, they are still prone to degradation. Oxidative lipid damage can also result in various products with truncated lipid tails ending with either an aldehyde or carboxylic group [37]. MD simulations showed that oxidized lipids with an aldehyde group disturb the bilayer more than the ones with a peroxide group, since the aldehyde lipid tails are significantly more mobile than the peroxide ones [39]. In bilayers with aldehyde-truncated tails also spontaneous pore formation was observed on the time scale of MD simulations (within a few hundred ns) which was in some severe cases followed by bilayer disintegration (micellation) [39,104–106]. On the contrary, such spontaneous pore formation was not observed in lipids containing a peroxide group [39,106]. Consistent with [39], we observed no spontaneous pore formation in our peroxidized systems.

The results from MD showing that pore formation and bilayer disintegration can be observed only in the presence of certain types of lipid oxidation products appear to be consistent with experimental findings. Experiments performed by Weber et al. [107] showed that giant unilamellar vesicles (GUVs) containing exclusively lipid hydroperoxide species preserve their membrane integrity, even when all of the lipids in the membrane are peroxidized. Similar was observed by Riske et al. [108] exploring GUVs with up to 60% lipid hydroperoxides. In contrast, Runas and Malmstadt [109] reported formation of pore defects in GUVs containing only 12.5% aldehyde-truncated 1-palmitoyl-2-(9′-oxo-nonanoyl)-sn-glycero-3-phosphocholine (POxnoPC). Spontaneous pore formation in GUVs was reported also by Sankhagowit et al. [110] under conditions which resulted in the production of aldehyde-truncated lipids.

Although experimental studies on electropermeabilized cells detected the presence of conjugated dienes [23–25], indicating that lipid hydroperoxides are indeed present, the studies also detected malondialdehyde [20,21,25], suggesting the presence of secondary oxidation products. High local concentrations of secondary peroxidation products could lead to spontaneous formation of small pores in the oxidatively damaged lesions. Such pores would be distinctly different from the electric-field-induced electropores in the non-oxidized parts of the lipid bilayer, specifically in terms of their lifetime. In contrast to electropores, which are expected to close on a nanosecond to microsecond time scale after the pulse, the spontaneously opened pores in oxidized membrane lesions could remain open until being repaired by cell membrane repair mechanisms. The idea that two distinct types of pores, transient pores and long-lived pores, govern the transmembrane transport was proposed by Pavlin et al. [91,92] following the studies of Neumann et al. [16]. While the transient pores can easily be identified with the electric-field-induced electropores, the molecular structure of the long-lived pores remained unidentified. Spontaneous formation of pores in oxidized membrane lesions offers a possible molecular basis for such long-lived pores.

Let us now return to the patch-clamp measurements of membrane conductance presented in Fig. 8 and estimate the number of pores that would result in the measured Δg:

$$N_p = \frac{\Delta g C_{cell}}{G_p} \tag{16}$$

where C_{cell} is the total capacitance of the cell membrane and G_p is the conductance of a single pore. The analytical approximation for the conductance of a cylindrical pore with radius r_p and length d is [111].

$$G_p = \frac{2\pi\sigma_p {r_p}^2}{\pi r_p + 2d} \tag{17}$$

where $\sigma_p = (\sigma_e - \sigma_i)/\ln(\sigma_e/\sigma_i)$ is the effective conductivity of the solution inside the pore with σ_e and σ_i denoting the extracellular and intracellular conductivity, respectively. When combining Eqs. (16) and (17) and inserting the parameter values relevant to the discussed experimental studies (C_{cell} = 6 pF [98], σ_e = 1.48 S/m [103], σ_i = 0.5 S/m, and d = 5 nm) it turns out that the conductance of a single pore with diameter of 1.5 nm (diameter of pores in oxidized bilayers estimated from MD [104,106]) is equivalent to Δg of ~0.04 nS/pF. In other words, the lowest and the highest measured values of Δg in Fig. 8 could be explained by formation of a single and few hundred pores, respectively. Few hundred pores with diameter of 1.5 nm would occupy only ~0.0001% of the cell membrane area. Formation of pores in oxidized membrane lesions could therefore reasonably account for the highest measured values of Δg.

5. Conclusions

We investigated whether the permeability and conductance of peroxidized bilayers is high enough to have a major contribution to the long-lived permeability and conductance of electropermeabilized cell membranes, which persists after application of electric pulses. For this purpose we calculated the permeability and conductance of bilayer patches containing hydroperoxide lipid derivatives and compared them to experimental measurements on electropermeabilized cells. Overall, our analysis indicates that the permeability and conductance of hydroperoxide lipid derivatives are sufficient to account for the lowest

measured values, but not high enough to reasonably explain the entire range of experimental measurements. Nevertheless, hydroperoxide lipid derivatives correspond to primary peroxidation products. Formation of lipid hydroperoxides can be followed by secondary lipid degradation, which results in cleavage of the lipid tails. Oxidatively damaged membrane lesions, which contain such fragmented oxidized lipids, could exhibit spontaneous pore formation. Such spontaneously-formed pores would have much longer lifetime than the electric-field-induced electropores in the non-oxidized parts of the lipid bilayer and could explain also the highest measured values of post-pulse permeability and conductance of electropermeabilized cell membranes. Whether such pores are formed in electropermeabilized membranes depends on the presence of secondary lipid peroxidation products and their local concentration within oxidized membrane lesions. Therefore, our study calls for experiments, which will determine the type and amount of lipid peroxidation products in electropermeabilized cell membranes. Such experiments coupled with theoretical analysis as presented in this study could give a definitive answer to the pertinent question: "What is the contribution of lipid peroxidation to membrane permeability in electropermeabilization?".

Funding sources

Part of the simulations was performed using HPC resources from the OCCIGEN center [(GENCI-CNRS) project number c2015077461]. This work was supported by Slovenian Research Agency (ARRS) [program P2-0249 and funding for Junior Researchers to L.R.], COST action TD1104 (www.electroporation.net) [Short Term Scientific MissionSTSM-TD1104-270215-057439]. M.T. Acknowledges the support from the "Contrat État Plan Region Lorraine 2015–2020" subproject MatDS.

Acknowledgements

The study was conducted in the scope of the European Associated Laboratory for Pulsed Electric Field Applications in Biology and Medicine (LEA EBAM). L.R. thanks P. E. Boukany for useful comments to the manuscript. The authors thank Michel A. Cuendet for help with the implementation and use of the dAFED/UFED code.

Appendix A. Supplementary data

Supplementary data to this article can be found online at https://doi.org/10.1016/j.bioelechem.2018.07.018.

References

[1] L. Rems, D. Miklavčič, Tutorial: electroporation of cells in complex materials and tissue, J. Appl. Phys. 119 (2016) 201101, https://doi.org/10.1063/1.4949264.
[2] M.L. Yarmush, A. Golberg, G. Serša, T. Kotnik, D. Miklavčič, Electroporation-based technologies for medicine: principles, applications, and challenges, Annu. Rev. Biomed. Eng. 16 (2014) 295–320, https://doi.org/10.1146/annurev-bioeng-071813-104622.
[3] C. Rosazza, S.H. Meglic, A. Zumbusch, M.-P. Rols, D. Miklavcic, Gene electrotransfer: a mechanistic perspective, Curr. Gene Ther. (2016) 98–129.
[4] H.J. Scheffer, K. Nielsen, M.C. de Jong, A.A.J.M. van Tilborg, J.M. Vieveen, A.R.A. Bouwman, S. Meijer, C. van Kuijk, P.M.P. van den Tol, M.R. Meijerink, Irreversible electroporation for nonthermal tumor ablation in the clinical setting: a systematic review of safety and efficacy, J. Vasc. Interv. Radiol. 25 (2014) 997–1011 , quiz 1011 https://doi.org/10.1016/j.jvir.2014.01.028.
[5] S. Toepfl, V. Heinz, D. Knorr, High intensity pulsed electric fields applied for food preservation, Chem. Eng. Process. Process Intensif. 46 (2007) 537–546, https://doi.org/10.1016/j.cep.2006.07.011.
[6] S. Mahnič-Kalamiza, E. Vorobiev, D. Miklavčič, Electroporation in food processing and biorefinery, J. Membr. Biol. 247 (2014) 1279–1304, https://doi.org/10.1007/s00232-014-9737-x.
[7] R. Benz, U. Zimmermann, The resealing process of lipid bilayers after reversible electrical breakdown, Biochim. Biophys. Acta Biomembr. 640 (1981) 169–178, https://doi.org/10.1016/0005-2736(81)90542-3.
[8] S. Kakorin, S.P. Stoylov, E. Neumann, Electro-optics of membrane electroporation in diphenylhexatriene-doped lipid bilayer vesicles, Biophys. Chem. 58 (1996) 109–116.
[9] K.C. Melikov, V.A. Frolov, A. Shcherbakov, A.V. Samsonov, Y.A. Chizmadzhev, L.V. Chernomordik, Voltage-induced nonconductive pre-pores and metastable single pores in unmodified planar lipid bilayer, Biophys. J. 80 (2001) 1829–1836.
[10] J.T. Sengel, M.I. Wallace, Imaging the dynamics of individual electropores, Proc. Natl. Acad. Sci. 113 (2016) 5281–5286, https://doi.org/10.1073/pnas.1517437113.
[11] J.C. Weaver, Y.A. Chizmadzhev, Theory of electroporation: a review, Bioelectrochem. Bioenerg. 41 (1996) 135–160.
[12] K.A. DeBruin, W. Krassowska, Modeling electroporation in a single cell. I. Effects Of field strength and rest potential, Biophys. J. 77 (1999) 1213–1224.
[13] D.P. Tieleman, The molecular basis of electroporation, BMC Biochem. 5 (2004) 10, https://doi.org/10.1186/1471-2091-5-10.
[14] M. Tarek, Membrane electroporation: a molecular dynamics simulation, Biophys. J. 88 (2005) 4045–4053.
[15] M.-P. Rols, J. Teissié, Electropermeabilization of mammalian cells. Quantitative analysis of the phenomenon, Biophys. J. 58 (1990) 1089–1098.
[16] E. Neumann, K. Toensing, S. Kakorin, P. Budde, J. Frey, Mechanism of electroporative dye uptake by mouse B cells, Biophys. J. 74 (1998) 98–108.
[17] A.G. Pakhomov, A.M. Bowman, B.L. Ibey, F.M. Andre, O.N. Pakhomova, K.H. Schoenbach, Lipid nanopores can form a stable, ion channel-like conduction pathway in cell membrane, Biochem. Biophys. Res. Commun. 385 (2009) 181–186, https://doi.org/10.1016/j.bbrc.2009.05.035.
[18] Z.A. Levine, P.T. Vernier, Life cycle of an electropore: field-dependent and field-independent steps in pore creation and annihilation, J. Membr. Biol. 236 (2010) 27–36, https://doi.org/10.1007/s00232-010-9277-y.
[19] W.F.D. Bennett, N. Sapay, D.P. Tieleman, Atomistic simulations of pore formation and closure in lipid bilayers, Biophys. J. 106 (2014) 210–219, https://doi.org/10.1016/j.bpj.2013.11.4486.
[20] S.-K. Yeo, M.-T. Liong, Effect of electroporation on viability and bioconversion of isoflavones in mannitol-soymilk fermented by lactobacilli and bifidobacteria, J. Sci. Food Agric. 93 (2013) 396–409, https://doi.org/10.1002/jsfa.5775.
[21] O. Yun, X.-A. Zeng, C.S. Brennan, Z. Han, Effect of pulsed electric field on membrane lipids and oxidative injury of *Salmonella typhimurium*, Int. J. Mol. Sci. 17 (2016) https://doi.org/10.3390/ijms17081374.
[22] U. Biedinger, R.J. Youngman, H. Schnabl, Differential effects of electrofusion and electropermeabilization parameters on the membrane integrity of plant protoplasts, Planta 180 (1990) 598–602, https://doi.org/10.1007/BF02411459.
[23] M. Maccarrone, N. Rosato, A.F. Agrò, Electroporation enhances cell membrane peroxidation and luminescence, Biochem. Biophys. Res. Commun. 206 (1995) 238–245, https://doi.org/10.1006/bbrc.1995.1033.
[24] M. Maccarrone, M.R. Bladergroen, N. Rosato, A.F. Agro, Role of lipid peroxidation in electroporation-induced cell permeability, Biochem. Biophys. Res. Commun. 209 (1995) 417–425, https://doi.org/10.1006/bbrc.1995.1519.
[25] L.C. Benov, P.A. Antonov, S.R. Ribarov, Oxidative damage of the membrane lipids after electroporation, Gen. Physiol. Biophys. 13 (1994) 85–97.
[26] M. Breton, L.M. Mir, Investigation of the chemical mechanisms involved in the electropulsation of membranes at the molecular level, Bioelectrochemistry 119 (2018) 76–83, https://doi.org/10.1016/j.bioelechem.2017.09.005.
[27] W. Zhao, R. Yang, Q. Liang, W. Zhang, X. Hua, Y. Tang, Electrochemical reaction and oxidation of lecithin under pulsed electric fields (PEF) processing, J. Agric. Food Chem. 60 (2012) 12204–12209, https://doi.org/10.1021/jf304236h.
[28] B. Gabriel, J. Teissie, Generation of reactive-oxygen species induced by electropermeabilization of Chinese hamster ovary cells and their consequence on cell viability, Eur. J. Biochem. 223 (1994) 25–33, https://doi.org/10.1111/j.1432-1033.1994.tb18962.x.
[29] B. Gabriel, J. Teissié, Spatial compartmentation and time resolution of photooxidation of a cell membrane probe in electropermeabilized Chinese hamster ovary cells, Eur. J. Biochem. 228 (1995) 710–718, https://doi.org/10.1111/j.1432-1033.1995.0710m.x.
[30] P. Bonnafous, M.-C. Vernhes, J. Teissié, B. Gabriel, The generation of reactive-oxygen species associated with long-lasting pulse-induced electropermeabilisation of mammalian cells is based on a non-destructive alteration of the plasma membrane, Biochim. Biophys. Acta Biomembr. 1461 (1999) 123–134, https://doi.org/10.1016/S0005-2736(99)00154-6.
[31] N. Sabri, B. Pelissier, J. Teissié, Electropermeabilization of intact maize cells induces an oxidative stress, Eur. J. Biochem. 238 (1996) 737–743, https://doi.org/10.1111/j.1432-1033.1996.0737w.x.
[32] O.N. Pakhomova, V.A. Khorokhorina, A.M. Bowman, R. Rodaitė-Riševičienė, G. Saulis, S. Xiao, A.G. Pakhomov, Oxidative effects of nanosecond pulsed electric field exposure in cells and cell-free media, Arch. Biochem. Biophys. 527 (2012) 55–64, https://doi.org/10.1016/j.abb.2012.08.004.
[33] H. Yin, L. Xu, N.A. Porter, Free radical lipid peroxidation: mechanisms and analysis, Chem. Rev. 111 (2011) 5944–5972, https://doi.org/10.1021/cr200084z.
[34] A. Reis, C.M. Spickett, Chemistry of phospholipid oxidation, Biochim. Biophys. Acta Biomembr. 1818 (2012) 2374–2387, https://doi.org/10.1016/j.bbamem.2012.02.002.
[35] K. Uchida, 4-Hydroxy-2-nonenal: a product and mediator of oxidative stress, Prog. Lipid Res. 42 (2003) 318–343, https://doi.org/10.1016/S0163-7827(03)00014-6.
[36] L.J. Marnett, Lipid peroxidation-DNA damage by malondialdehyde, Mutat. Res. 424 (1999) 83–95http://www.ncbi.nlm.nih.gov/pubmed/10064852.
[37] P. Jurkiewicz, A. Olżyńska, L. Cwiklik, E. Conte, P. Jungwirth, F.M. Megli, M. Hof, Biophysics of lipid bilayers containing oxidatively modified phospholipids: insights from fluorescence and EPR experiments and from MD simulations, Biochim. Biophys. Acta 1818 (2012) 2388–2402.
[38] J. Wong-Ekkabut, Z. Xu, W. Triampo, I.-M. Tang, D.P. Tieleman, L. Monticelli, Effect of lipid peroxidation on the properties of lipid bilayers: a molecular dynamics

study, Biophys. J. 93 (2007) 4225–4236, https://doi.org/10.1529/biophysj.107.112565.
[39] P. Boonnoy, V. Jarerattanachat, M. Karttunen, J. Wong-ekkabut, Bilayer deformation, pores, and micellation induced by oxidized lipids, J. Phys. Chem. Lett. (2015) 4884–4888, https://doi.org/10.1021/acs.jpclett.5b02405.
[40] P.T. Vernier, Z.A. Levine, Y.-H. Wu, V. Joubert, M.J. Ziegler, L.M. Mir, D.P. Tieleman, Electroporating fields target oxidatively damaged areas in the cell membrane, PLoS One 4 (2009), e7966. https://doi.org/10.1371/journal.pone.0007966.
[41] M. Leguèbe, A. Silve, L.M. Mir, C. Poignard, Conducting and permeable states of cell membrane submitted to high voltage pulses: mathematical and numerical studies validated by the experiments, J. Theor. Biol. 360 (2014) 83–94, https://doi.org/10.1016/j.jtbi.2014.06.027.
[42] J. Teissié, T.Y. Tsong, Evidence of voltage-induced channel opening in Na/K ATPase of human erythrocyte membrane, J. Membr. Biol. 55 (1980) 133–140, https://doi.org/10.1007/BF01871155.
[43] J. Teissié, M. Golzio, M.-P. Rols, Mechanisms of cell membrane electropermeabilization: a minireview of our present (lack of ?) knowledge, Biochim. Biophys. Acta, Gen. Subj. 1724 (2005) 270–280, https://doi.org/10.1016/j.bbagen.2005.05.006.
[44] A. Azan, V. Untereiner, L. Descamps, C. Merla, C. Gobinet, M. Breton, O. Piot, L.M. Mir, Comprehensive characterization of the interaction between pulsed electric fields and live cells by confocal Raman microspectroscopy, Anal. Chem. 89 (2017) 10790–10797, https://doi.org/10.1021/acs.analchem.7b02079.
[45] L.H. Wegner, W. Frey, A. Silve, Electroporation of DC-3F cells is a dual process, Biophys. J. 108 (2015) 1660–1671, https://doi.org/10.1016/j.bpj.2015.01.038.
[46] E. Niki, Y. Yoshida, Y. Saito, N. Noguchi, Lipid peroxidation: mechanisms, inhibition, and biological effects, Biochem. Biophys. Res. Commun. 338 (2005) 668–676, https://doi.org/10.1016/j.bbrc.2005.08.072.
[47] S.K. Abbott, P.L. Else, T.A. Atkins, A.J. Hulbert, Fatty acid composition of membrane bilayers: importance of diet polyunsaturated fat balance, Biochim. Biophys. Acta Biomembr. 1818 (2012) 1309–1317, https://doi.org/10.1016/j.bbamem.2012.01.011.
[48] N.A. Busch, M.L. Yarmush, M. Toner, A theoretical formalism for aggregation of peroxidized lipids and plasma membrane stability during photolysis, Biophys. J. 75 (1998) 2956–2970, https://doi.org/10.1016/S0006-3495(98)77737-9.
[49] E. Lindahl, P. Bjelkmar, P. Larsson, M.A. Cuendet, B. Hess, Implementation of the CHARMM force field in GROMACS: Analysis of protein stability effects from correction maps, virtual interaction sites, and water models, J. Chem. Theory Comput. 6 (2010) 459–466.
[50] J.B. Klauda, R.M. Venable, J.A. Freites, J.W. O'Connor, D.J. Tobias, C. Mondragon-Ramirez, I. Vorobyov, A.D. MacKerell, R.W. Pastor, Update of the CHARMM all-atom additive force field for lipids: validation on six lipid types, J. Phys. Chem. B 114 (2010) 7830–7843, https://doi.org/10.1021/jp101759q.
[51] T.J. Piggot, Á. Piñeiro, S. Khalid, Molecular dynamics simulations of phosphatidylcholine membranes: a comparative force field study, J. Chem. Theory Comput. 8 (2012) 4593–4609, https://doi.org/10.1021/ct3003157.
[52] J. Garrec, A. Monari, X. Assfeld, L.M. Mir, M. Tarek, Lipid peroxidation in membranes: the peroxyl radical does not "float", J. Phys. Chem. Lett. 5 (2014) 1653–1658.
[53] W.L. Jorgensen, J. Chandrasekhar, J.D. Madura, R.W. Impey, M.L. Klein, Comparison of simple potential functions for simulating liquid water, J. Chem. Phys. 79 (1983) 926 (http://scitation.aip.org/content/aip/journal/jcp/79/2/10.1063/1.445869$\$nhttp://link.aip.org/link/?JCPSA6/79/926/1).
[54] I. Leontyev, A. Stuchebrukhov, Accounting for electronic polarization in non-polarizable force fields, Phys. Chem. Chem. Phys. 13 (2011) 2613–2626, https://doi.org/10.1039/C0CP01971B.
[55] M. Kohagen, P.E. Mason, P. Jungwirth, Accurate description of calcium solvation in concentrated aqueous solutions, J. Phys. Chem. B 118 (2014) 7902–7909, https://doi.org/10.1021/jp5005693.
[56] M. Kohagen, P.E. Mason, P. Jungwirth, Accounting for electronic polarization effects in aqueous sodium chloride via molecular dynamics aided by neutron scattering, J. Phys. Chem. B 120 (2016) 1454–1460, https://doi.org/10.1021/acs.jpcb.5b05221.
[57] B. Hess, C. Kutzner, D. van der Spoel, E. Lindahl, GROMACS 4: algorithms for highly efficient, load-balanced, and scalable molecular simulation, J. Chem. Theory Comput. 4 (2008) 435–447, https://doi.org/10.1021/ct700301q.
[58] H.J.C. Berendsen, J.P.M. Postma, W.F. van Gunsteren, A. DiNola, J.R. Haak, Molecular dynamics with coupling to an external bath, J. Chem. Phys. 81 (1984) 3684–3690, https://doi.org/10.1063/1.448118.
[59] S. Nosé, A molecular dynamics method for simulations in the canonical ensemble, Mol. Phys. 52 (1984) 255–268 (http://www.tandfonline.com/doi/abs/10.1080/00268978400101201$\$nhttp://www.tandfonline.com/doi/pdf/10.1080/00268978400101201).
[60] W.G. Hoover, Canonical dynamics: equilibrium phase-space distributions, Phys. Rev. A 31 (1985) 1695–1697.
[61] M. Parrinello, A. Rahman, Polymorphic transitions in single crystals: a new molecular dynamics method, J. Appl. Phys. 52 (1981) 7182–7190, https://doi.org/10.1063/1.328693.
[62] S. Nosé, M.L. Klein, Constant pressure molecular dynamics for molecular systems, Mol. Phys. 50 (1983) 1055–1076, https://doi.org/10.1080/00268978300102851.
[63] T. Darden, D. York, L. Pedersen, Particle mesh Ewald: an N·log(N) method for Ewald sums in large systems, J. Chem. Phys. 98 (1993) 10089–10092, https://doi.org/10.1063/1.464397.
[64] B. Hess, H. Bekker, H.J.C. Berendsen, J.G.E.M. Fraaije, LINCS: a linear constraint solver for molecular simulations, J. Comput. Chem. 18 (1997) 1463–1472, https://doi.org/10.1002/(SICI)1096-987X(199709)18:12<1463::AID-JCC4>3.0.CO;2-H.
[65] V. Jarerattanachat, M. Karttunen, J. Wong-Ekkabut, Molecular dynamics study of oxidized lipid bilayers in NaCl solution, J. Phys. Chem. B 117 (2013) 8490–8501.
[66] W. Humphrey, A. Dalke, K. Schulten, VMD: visual molecular dynamics, J. Mol. Graph. 14 (1996) 33–38, https://doi.org/10.1016/0263-7855(96)00018-5.
[67] M. Chen, M.A. Cuendet, M.E. Tuckerman, Heating and flooding: a unified approach for rapid generation of free energy surfaces, J. Chem. Phys. 137 (2012) 24102, https://doi.org/10.1063/1.4733389.
[68] M.A. Cuendet, M.E. Tuckerman, Free energy reconstruction from metadynamics or adiabatic free energy dynamics simulations, J. Chem. Theory Comput. 10 (2014) 2975–2986, https://doi.org/10.1021/ct500012b.
[69] J.B. Abrams, M.E. Tuckerman, Efficient and direct generation of multidimensional free energy surfaces via adiabatic dynamics without coordinate transformations, J. Phys. Chem. B 112 (2008) 15742–15757, https://doi.org/10.1021/jp805039u.
[70] L. Maragliano, E. Vanden-Eijnden, A temperature accelerated method for sampling free energy and determining reaction pathways in rare events simulations, Chem. Phys. Lett. 426 (2006) 168–175, https://doi.org/10.1016/j.cplett.2006.05.062.
[71] A. Laio, M. Parrinello, Escaping free-energy minima, Proc. Natl. Acad. Sci. U. S. A. 99 (2002) 12562–12566, https://doi.org/10.1073/pnas.202427399.
[72] A. Barducci, M. Bonomi, M. Parrinello, Metadynamics, Wiley Interdiscip. Rev. Comput. Mol. Sci. 1 (2011) 826–843, https://doi.org/10.1002/wcms.31.
[73] M. Bonomi, D. Branduardi, G. Bussi, C. Camilloni, D. Provasi, P. Raiteri, D. Donadio, F. Marinelli, F. Pietrucci, R.A. Broglia, M. Parrinello, PLUMED: a portable plugin for free-energy calculations with molecular dynamics, Comput. Phys. Commun. 180 (2009) 1961–1972, https://doi.org/10.1016/j.cpc.2009.05.011.
[74] M.A. Cuendet, PLUMED User's Guide, Complement for the dAFED and UFED methods, 2012.
[75] I. Vorobyov, T.E. Olson, J.H. Kim, R.E. Koeppe, O.S. Andersen, T.W. Allen, Ion-induced defect permeation of lipid membranes, Biophys. J. 106 (2014) 586–597, https://doi.org/10.1016/j.bpj.2013.12.027.
[76] G. Hummer, Position-dependent diffusion coefficients and free energies from Bayesian analysis of equilibrium and replica molecular dynamics simulations, New J. Phys. 7 (2005) 34, https://doi.org/10.1088/1367-2630/7/1/034.
[77] S.-J. Marrink, H.J.C. Berendsen, Simulation of water transport through a lipid membrane, J. Phys. Chem. 98 (1994) 4155–4168, https://doi.org/10.1021/j100066a040.
[78] O.S. Andersen, M. Fuchs, Potential energy barriers to ion transport within lipid bilayers. Studies with tetraphenylborate, Biophys. J. 15 (1975) 795–830, https://doi.org/10.1016/S0006-3495(75)85856-5.
[79] R.P. Mason, M.F. Walter, P.E. Mason, Effect of oxidative stress on membrane structure: small-angle X-ray diffraction analysis, Free Radic. Biol. Med. 23 (1997) 419–425, https://doi.org/10.1016/S0891-5849(97)00101-9.
[80] L. Wang, P.S. Bose, F.J. Sigworth, Using cryo-EM to measure the dipole potential of a lipid membrane, Proc. Natl. Acad. Sci. 103 (2006) 18528–18533.
[81] I.V. Khavrutskii, A.A. Gorfe, B. Lu, J.A. McCammon, Free energy for the permeation of Na+ and Cl− Ions and their ion-pair through a zwitterionic dimyristoyl phosphatidylcholine lipid bilayer by umbrella integration with harmonic Fourier beads, J. Am. Chem. Soc. 131 (2009) 1706–1716, https://doi.org/10.1021/ja8081704.
[82] D. Papahadjopoulos, S. Nir, S. Ohki, Permeability properties of phospholipid membranes: effect of cholesterol and temperature, Biochim. Biophys. Acta Biomembr. 266 (1972) 561–583, https://doi.org/10.1016/0005-2736(72)90354-9.
[83] H. Hauser, M.C. Phillips, M. Stubbs, Ion permeability of phospholipid bilayers, Nature 239 (1972) 342, https://doi.org/10.1038/239342a0.
[84] H. Hauser, D. Oldani, M.C. Phillips, Mechanism of ion escape from phosphatidylcholine and phosphatidylserine single bilayer vesicles, Biochemistry 12 (1973) 4507–4517, https://doi.org/10.1021/bi00746a032.
[85] S. Paula, A.G. Volkov, D.W. Deamer, Permeation of halide anions through phospholipid bilayers occurs by the solubility-diffusion mechanism, Biophys. J. 74 (1998) 319–327, https://doi.org/10.1016/S0006-3495(98)77789-6.
[86] T. Hanai, D.A. Haydon, J. Taylor, The variation of capacitance and conductance of bimolecular lipid membranes with area, J. Theor. Biol. 9 (1965) 433–443, https://doi.org/10.1016/0022-5193(65)90042-1.
[87] R. Shirakashi, V.L. Sukhorukov, I. Tanasawa, U. Zimmermann, Measurement of the permeability and resealing time constant of the electroporated mammalian cell membranes, Int. J. Heat Mass Transf. 47 (2004) 4517–4524, https://doi.org/10.1016/j.ijheatmasstransfer.2004.04.007.
[88] A.A. Gurtovenko, I. Vattulainen, Effect of NaCl and KCl on phosphatidylcholine and phosphatidylethanolamine lipid membranes: insight from atomic-scale simulations for understanding salt-induced effects in the plasma membrane, J. Phys. Chem. B 112 (2008) 1953–1962.
[89] H. Binder, O. Zschörnig, The effect of metal cations on the phase behavior and hydration characteristics of phospholipid membranes, Chem. Phys. Lipids 115 (2002) 39–61, https://doi.org/10.1016/S0009-3084(02)00005-1.
[90] B. Alberts, A. Johnson, J. Lewis, M. Raff, K. Roberts, P. Walter, Molecular Biology of the Cell, Garland Science, New York; Abingdon, UK, 2008.
[91] M. Pavlin, V. Leben, D. Miklavčič, Electroporation in dense cell suspension—theoretical and experimental analysis of ion diffusion and cell permeabilization, Biochim. Biophys. Acta, Gen. Subj. 1770 (2007) 12–23, https://doi.org/10.1016/j.bbagen.2006.06.014.
[92] M. Pavlin, D. Miklavčič, Theoretical and experimental analysis of conductivity, ion diffusion and molecular transport during cell electroporation — relation between short-lived and long-lived pores, Bioelectrochemistry 74 (2008) 38–46, https://doi.org/10.1016/j.bioelechem.2008.04.016.
[93] M. Pavlin, M. Kandušer, M. Reberšek, G. Pucihar, F.X. Hart, R. Magjarevićcacute, D. Miklavčič, Effect of cell electroporation on the conductivity of a cell suspension, Biophys. J. 88 (2005) 4378–4390, https://doi.org/10.1529/biophysj.104.048975.
[94] T.Y. Tsong, Electroporation of cell membrane, Biophys. J. 60 (1991) 297–306.

[96] E.K. Hoffmann, I.H. Lambert, S.F. Pedersen, Physiology of cell volume regulation in vertebrates, Physiol. Rev. 89 (2009) 193–277, https://doi.org/10.1152/physrev.00037.2007.
[97] A.G. Pakhomov, J.F. Kolb, J.A. White, R.P. Joshi, S. Xiao, K.H. Schoenbach, Long-lasting plasma membrane permeabilization in mammalian cells by nanosecond pulsed electric field (nsPEF), Bioelectromagnetics 28 (2007) 655–663, https://doi.org/10.1002/bem.20354.
[98] A.G. Pakhomov, R. Shevin, J.A. White, J.F. Kolb, O.N. Pakhomova, R.P. Joshi, K.H. Schoenbach, Membrane permeabilization and cell damage by ultrashort electric field shocks, Arch. Biochem. Biophys. 465 (2007) 109–118, https://doi.org/10.1016/j.abb.2007.05.003.
[99] B.L. Ibey, D.G. Mixon, J.A. Payne, A. Bowman, K. Sickendick, G.J. Wilmink, W.P. Roach, A.G. Pakhomov, Plasma membrane permeabilization by trains of ultrashort electric pulses, Bioelectrochemistry 79 (2010) 114–121, https://doi.org/10.1016/j.bioelechem.2010.01.001.
[100] K. Asami, Y. Takahashi, S. Takashima, Frequency domain analysis of membrane capacitance of cultured cells (HeLa and myeloma) using the micropipette technique, Biophys. J. 58 (1990) 143–148.
[101] V.L. Sukhorukov, W.M. Arnold, U. Zimmermann, Hypotonically induced changes in the plasma membrane of cultured mammalian cells, J. Membr. Biol. 132 (1993) 27–40, https://doi.org/10.1007/BF00233049.
[102] *Vasyl Nesin, Angela M. Bowman, Shu Xiao, Andrei G. Pakhomov, Cell permeabilization and inhibition of voltage-gated Ca2+ and Na+ channel currents by nanosecond pulsed electric fields, Bioelectromagnetics 33 (2012) 394–404, https://doi.org/10.1002/bem.21696.
[103] B.L. Ibey, S. Xiao, K.H. Schoenbach, M.R. Murphy, A.G. Pakhomov, Plasma membrane permeabilization by 60- and 600-ns electric pulses is determined by the absorbed dose, Bioelectromagnetics 30 (2009) 92–99, https://doi.org/10.1002/bem.20451.
[104] L. Cwiklik, P. Jungwirth, Massive oxidation of phospholipid membranes leads to pore creation and bilayer disintegration, Chem. Phys. Lett. 486 (2010) 99–103, https://doi.org/10.1016/j.cplett.2010.01.010.
[105] M. Lis, A. Wizert, M. Przybylo, M. Langner, J. Swiatek, P. Jungwirth, L. Cwiklik, The effect of lipid oxidation on the water permeability of phospholipids bilayers, Phys. Chem. Chem. Phys. 13 (2011) 17555–17563, https://doi.org/10.1039/c1cp21009b.
[106] J. Van der Paal, E.C. Neyts, C.C.W. Verlackt, A. Bogaerts, Effect of lipid peroxidation on membrane permeability of cancer and normal cells subjected to oxidative stress, Chem. Sci. 7 (2015) 489–498, https://doi.org/10.1039/C5SC02311D.
[107] G. Weber, T. Charitat, M.S. Baptista, A.F. Uchoa, C. Pavani, H.C. Junqueira, Y. Guo, V.A. Baulin, R. Itri, C.M. Marques, A.P. Schroder, Lipid oxidation induces structural changes in biomimetic membranes, Soft Matter 10 (2014) 4241–4247, https://doi.org/10.1039/C3SM52740A.
[108] K.A. Riske, T.P. Sudbrack, N.L. Archilha, A.F. Uchoa, A.P. Schroder, C.M. Marques, M.S. Baptista, R. Itri, Giant vesicles under oxidative stress induced by a membrane-anchored photosensitizer, Biophys. J. 97 (2009) 1362–1370, https://doi.org/10.1016/j.bpj.2009.06.023.
[109] K.A. Runas, N. Malmstadt, Low levels of lipid oxidation radically increase the passive permeability of lipid bilayers, Soft Matter 11 (2015) 499–505, https://doi.org/10.1039/c4sm01478b.
[110] S. Sankhagowit, S.-H. Wu, R. Biswas, C.T. Riche, M.L. Povinelli, N. Malmstadt, The dynamics of giant unilamellar vesicle oxidation probed by morphological transitions, Biochim. Biophys. Acta Biomembr. 1838 (2014) 2615–2624, https://doi.org/10.1016/j.bbamem.2014.06.020.
[111] J. Li, H. Lin, The current-voltage relation for electropores with conductivity gradients, Biomicrofluidics 4 (2010) 13206, https://doi.org/10.1063/1.3324847.